Available online at www.sciencedirect.com
ScienceDirect
Polymer 47 (2006) 7485–7496
polymer
www.elsevier.com/locate/polymer

Supercritical CO_2 dispersion of nano-clays and clay/polymer nanocomposites

Steven Horsch, Gulay Serhatkulu, Esin Gulari, Rangaramanujam M. Kannan*

Department of Chemical Engineering and Materials Science, Wayne State University, 1121 Engineering, 5050 Anthony Wayne Drive, Detroit, MI 48202, USA

Received 21 April 2006; received in revised form 19 August 2006; accepted 21 August 2006
Available online 12 September 2006

Abstract

Dispersed polymer/clay nanocomposites are of great interest because they can significantly improve the properties of existing polymeric materials. However, achieving a high level of clay dispersion has been a key challenge in the production of polymer/clay nanocomposites. In this paper, we explore a novel supercritical carbon dioxide ($scCO_2$) processing method that utilizes $scCO_2$ to disperse nano-clays. The structure and properties of the clays and the resultant nanocomposites are characterized using a combination of wide-angle X-ray diffraction (WAXD), scanning electron microscopy (SEM), transmission electron microscopy (TEM), and rheology. Significant dispersion was achieved with dry Cloisite 93A clay, whereas relatively poor dispersion was achieved with dry Cloisite Na^+ (natural clay). The extent of clay dispersion appears to be dependent on the 'CO_2-philicity', which in turn appears to depend on the surface modifications and inter-gallery spacing. The presence of an acidic hydrogen on the surfactant in Cloisite 93A appears to play a strong role in its 'CO_2-philicity'. The ability to delaminate dry clays is significant because it will likely increase the ability to produce dispersed clay/polymer nanocomposites via melt processing. In addition to delaminating dry clays, we demonstrate that CO_2-phobic Cloisite Na^+ (natural clay) can be partially dispersed with $scCO_2$, using a CO_2-philic polymer, polydimethylsiloxane (PDMS). The dispersed clay/PDMS nanocomposite shows an order of magnitude increase in the dynamic storage modulus at low frequencies, accompanied by the emergence of a 'solid-like' plateau, characteristic of dispersed nanocomposites with enhanced clay/polymer interactions.

Keywords: Nanocomposites; Supercritical carbon dioxide; Nano-clays

1. Introduction

Over the past decade considerable effort has been put forth to disperse/exfoliate nano-clays in polymers. This is due to their potential for remarkable enhancements in polymer properties. These benefits include improved tensile strength [1], decreased gas permeability [2,3], thermal stability, and improved flame retardancy [4]. A key to several of the improvements is the large interfacial area generated when the nano-clays are intercalated or exfoliated [5–14]. However, dispersing the nano-clay stacks into individual layers is still a challenge. The starting point for most montmorillonite-based nanocomposites is surface modification of the natural clay with alkylammonium or phosphonium cations that increase the inter-gallery spacing and render the clay organo-philic [15]. The modified or organo-philic clay can then be dispersed in an appropriate polymer matrix by a variety of methods. These methods can be broken down into three categories: intercalation of prepolymer or polymer from solution, melt intercalation, and *in situ* intercalative polymerization. A wide range of nanocomposites have been formed by melt mixing, solution casting, and *in situ* polymerization. Melt mixing and solution casting primarily result in intercalated nanocomposites, and *in situ* polymerization provides a range of dispersion from intercalated to exfoliated [16–25]. Although all of these methods have been somewhat effective in producing nanocomposites, from a processing stand point, melt intercalation is likely the most viable

* Corresponding author. Tel.: +1 313 577 3879; fax: +1 313 577 3810.
E-mail address: rkannan@chem1.eng.wayne.edu (R.M. Kannan).

0032-3861/$ - see front matter © 2006 Elsevier Ltd. All rights reserved.
doi:10.1016/j.polymer.2006.08.048

method for producing nanocomposites at an industrial level. Therefore, it would be advantageous to develop methods that augment melt processing and help to increase the extent of nano-clay dispersion.

Recently, supercritical fluids (SCFs) have received a great deal of attention and are currently being used as environmentally friendly solvents for a range of materials synthesis and process applications including polymerization, polymer purification and fractionation, coating applications, and powder formation [26]. In general, SCFs offer mass transfer advantages over conventional organic solvents because of their ''gas-like'' diffusivity, liquid-like density, low viscosity, and surface tension [26–28]. In particular, supercritical carbon dioxide ($scCO_2$) has emerged as an important SCF due to its many desirable attributes such as low cost, abundance, low toxicity, and readily accessible supercritical conditions ($T_c = 31.1$ °C, $P_c = 7.38$ MPa, $\rho_c = 0.472$ g/mL). When CO_2 is raised above its critical point, its physicochemical properties can be continuously tuned between vapor-like and liquid-like limits by varying the system pressure and/or temperature. Moreover, it has been shown that a variety of polymers exhibit solubility in SCFs and that the extent of solubility depends on the molecular weight of the polymers and the processing conditions. Silicones (*e.g.*, polydimethylsiloxane – PDMS) and fluorinated hydrocarbons exhibit miscibility at pressures well below alkanes of comparable chain length in CO_2 [29–32].

In this paper we present a novel method, which exploits the physicochemical properties of supercritical carbon dioxide ($scCO_2$) to disperse and/or coat nano-clays for use in polymeric nanocomposites [33,34]. The dispersion is discussed in the context of clay surface modification and CO_2-philicity. Specifically, we demonstrate the ability of $scCO_2$ processing to delaminate CO_2-philic nano-clays in their dry state and show that the type of surface modification impacts the CO_2-philicity of the nano-clay and hence the extent of delamination. In addition, we demonstrate the ability of a CO_2-philic polymer to aid in the dispersion of a ''CO_2-phobic'' natural clay (Cloisite Na^+). The matrix polymer for the nanocomposites, polydimethylsiloxane (PDMS), was chosen because of its well documented miscibility with $scCO_2$ and because it has a Si–O backbone, which may interact favorably with the silicate surface of natural montmorillonite [35–37]. In addition, clay loadings of 15 wt% were used to determine the feasibility of producing highly loaded master-batches using $scCO_2$, for further compounding. The structure and mechanical properties of the nano-clays and nanocomposites have been investigated via electron microscopy, wide-angle X-ray diffraction (WAXD), and rheology. The properties of the resultant nanocomposites are compared to analogous materials from literature.

2. Experimental methods

2.1. Materials

The Cloisite series of clays 93A, 15A, and Na^+ used in this study were obtained from Southern Clay Products. The I.30P was provided by Nanocor. The composition and physical properties of the nano-clays are summarized in Table 1. The cation exchange capacities (CEC) of all the clays have been reported by the manufacturers to be 92.6 mequiv/100 g. The two PDMS samples are polydisperse, with weight-average molecular weights of 39,000 g/mol and 400,000 g/mol, and were purchased from Scientific Polymer Products, Inc.

Table 1
Nano-clay composition

Name	Organic modifier	d_{001} spacing (nm)
Cloisite Na^+	None	1.17
Cloisite 93A	*Methyl* dihydrogenated tallow	2.36
Cloisite 15A	*Dimethyl* dihydrogenated tallow	3.15
I.30P	*Trimethyl* hydrogenated tallow	2.3

2.2. $scCO_2$ processing

The $scCO_2$ processing method involves contacting nano-clays or polymer nano-clay mixtures with $scCO_2$. The process is shown pictorially in Fig. 1. The layered nano-clays or polymer/clay mixtures are contacted with CO_2 in a high pressure vessel (A); the system is then raised above the critical point for CO_2 and the material is allowed to soak for an appropriate time (B); the system is then rapidly depressurized to atmospheric pressure (C). A preliminary hypothesis for the mechanism is: during the soak step (B), under the selected processing conditions, the CO_2 or the mixture of the CO_2 and polymer diffuses between the clay layers. In the case where polymer is present, the high diffusivity and low viscosity of the CO_2-philic polymer in the mixture enables clay layer penetration. In the case where only CO_2 and clay are present the CO_2 diffuses into the CO_2-philic clay gallery. During depressurization, expansion of the $scCO_2$ between the layers pushes them apart resulting in delaminated nanocomposites or nano-clays. When the CO_2 is completely removed a good portion of the nano-clay platelets remain separated or in the case where polymer is present the organic material remains between the layers, coating the surfaces of the layers, thus preventing reformation of the layered structure.

2.2.1. $scCO_2$ dispersion of pure nano-clays

The four different nano-clays (Cloisite 93A, Cloisite 15A, Cloisite Na^+ (natural clay), and I.30P) were processed in

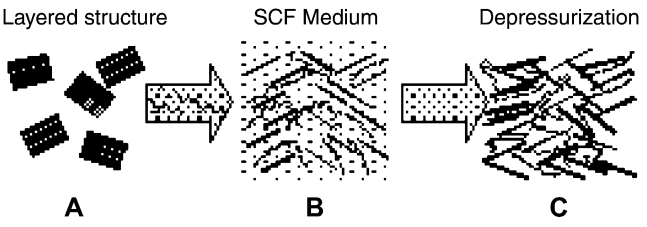

Fig. 1. Supercritical Fluid Processing. In step (A) the silicate and host polymer are mixed and the resulting composite is placed in the processing vessel. In step (B) the vessel is pressurized with $scCO_2$ and then heated. In step (C) the vessel is rapidly depressurized.

$scCO_2$ at 90 °C and 8.6 MPa, which corresponds to a CO_2 density of 0.157 g/cm^3. The clay was allowed to soak in $scCO_2$ for 20 h under quiescent conditions; at which time, the system was rapidly depressurized. The structure and morphology of the processed clays were then studied via WAXD and scanning electron microscopy (SEM).

2.2.2. Formation of nanocomposites

The nanocomposites formed via the *$scCO_2$* processing method were produced by hand mixing the *as-received* Cloisite Na^+ with either high molecular weight PDMS or a blend of low and high molecular weight PDMS (20 wt% 39K, 80 wt% 400K) until the nano-clay was coated with the polymer. This is easily accomplished because of the soft, liquid-like properties of PDMS at room temperature. The mixture is then processed in *$scCO_2$* under appropriate conditions to form the nanocomposite. During the *$scCO_2$* process, the high mobility of the polymer and the rapid depressurization are expected to facilitate uniform distribution and dispersion of the nano-clay in the host polymer matrix. These nanocomposites are benchmarked against composites made by mechanically mixing the appropriate amount of as-received nano-clay with the appropriate PDMS and annealing at 90 °C in a vacuum oven for 24 h. This annealing time is comparable to those used for $scCO_2$ processing, thus ruling out any role of thermal annealing in the enhanced properties achieved during $scCO_2$ processing.[1] The mechanical mixing of the nano-clay with the PDMS was carried out in a 256 mL Thar vessel equipped with a variable speed impeller. The nano-clay and PDMS were mixed for 2 h at low impeller speeds and 25 °C to uniformly distribute the nano-clay throughout the polymer matrix followed by the annealing step to further promote intercalation of polymer chains into the inter-gallery of the nano-clay. The composition, processing method and processing conditions for the nanocomposites are shown in Table 2.

2.3. Wide-angle X-ray diffraction (WAXD)

WAXD was used to determine the inter-gallery spacing of the *as-received* clays, *$scCO_2$ processed* clays, and clay/polymer nanocomposites. The d_{001} spacing for the clays was determined using the JADE software accompanying the diffractometer. The inter-gallery spacing was calculated by subtracting 1 nm (platelet thickness) from the d_{001} spacing. All data were collected using a Rigaku Rotaflex powder diffractometer with a Cu Kα X-ray source ($\lambda = 1.54$ Å) and an accelerating voltage of 40 kV at a current of 150 mA. To perform scans, samples were placed in a custom made zero background quartz sample-holder that is 0.9 mm in depth. Scans were carried out in different orientations of a sample and different locations in the sample and verified to be reproducible when diffraction patterns were superimposed on one another.

[1] For all the samples discussed in this paper, we do not observe any mass change upon $scCO_2$ processing, suggesting no PDMS loss.

Table 2
Nanocomposite composition

Sample	Polymer (M_w)	Clay	wt% filler	Processing conditions[a]
$PDMS_{400K}$(BM)	400K	Cloisite Na^+	15	1,4
$PDMS_{400K}$(sc)	400K	Cloisite Na^+	15	1,2
$PDMS_{blend}$(sc)	20 wt% 39K, 80 wt% 400K	Cloisite Na^+	15	1,3

[a] 1, Mechanical mixing of clay and polymer prior to processing; 2, $scCO_2$ processing at 27.6 MPa and 50 °C for 24 h; 3, $scCO_2$ processing at 13.78 MPa and 50 °C for 24 h; 4, annealed at 90 °C for 24 h.

2.4. Electron microscopy (SEM and TEM)

SEM was used to understand the morphology of nano-clays before and after *$scCO_2$ processing*. Images were collected using a Hitachi S-2400 scanning electron microscope with an electron potential of 25 kV. Many (10–20) images were collected for all samples to ensure accurate representation of the clay structure. *Transmission electron microscopy* (TEM) was used to investigate the clay structure in the PDMS matrix. Thin films of the nanocomposites were prepared by a compression molding technique. The films were cut into pieces and placed between Teflon sheets at 80 °C and compressed to form thinner films. This process was repeated to achieve a film thickness that would allow for imaging. The films were removed using liquid nitrogen and placed on 200 mesh carbon film coated copper grids. The samples were examined with a JEOL FastEM 2010 HR TEM operated at 200 kV.

2.5. Rheology

Melt rheological measurements were performed under oscillatory shear using an RSA II rheometer (shear sandwich geometry $15.98 \times 12.7 \times 0.55$ mm^3). Measurements were performed at a single temperature for PDMS nanocomposites because of the very small time–temperature superposition shift factors associated with PDMS at room temperature ($T_g \sim -128$ °C). The experimental frequency range was $0.01 \leq \omega \leq 100$ rad s^{-1} for all samples. The samples were loaded, compressed and allowed to equilibrate for 1 h at the desired temperature.[2] Linear viscoelastic measurements were made at low strains ($\gamma_o < 0.07$) and strain sweeps were performed to ensure that the dynamic moduli were independent of the strains utilized. *Steady shear viscosity* measurements were carried out on a Rheometrics ARES rheometer with a transducer capable of torque measurements over a range from 0.2–2000 g cm. Viscosity measurements were carried out at a single temperature of 25 °C with a cone angle of 0.1 rad, a plate diameter of 25 mm, and a gap of 0.05 mm. Steady shear measurements were done by applying a strain rate ranging from 0.01–100 s^{-1}.

[2] This is a typical equilibration time we use in rheology, to allow the temperature to reach the set point. In the RSA II instrument it takes greater than 20–30 min, depending on the temperature jump.

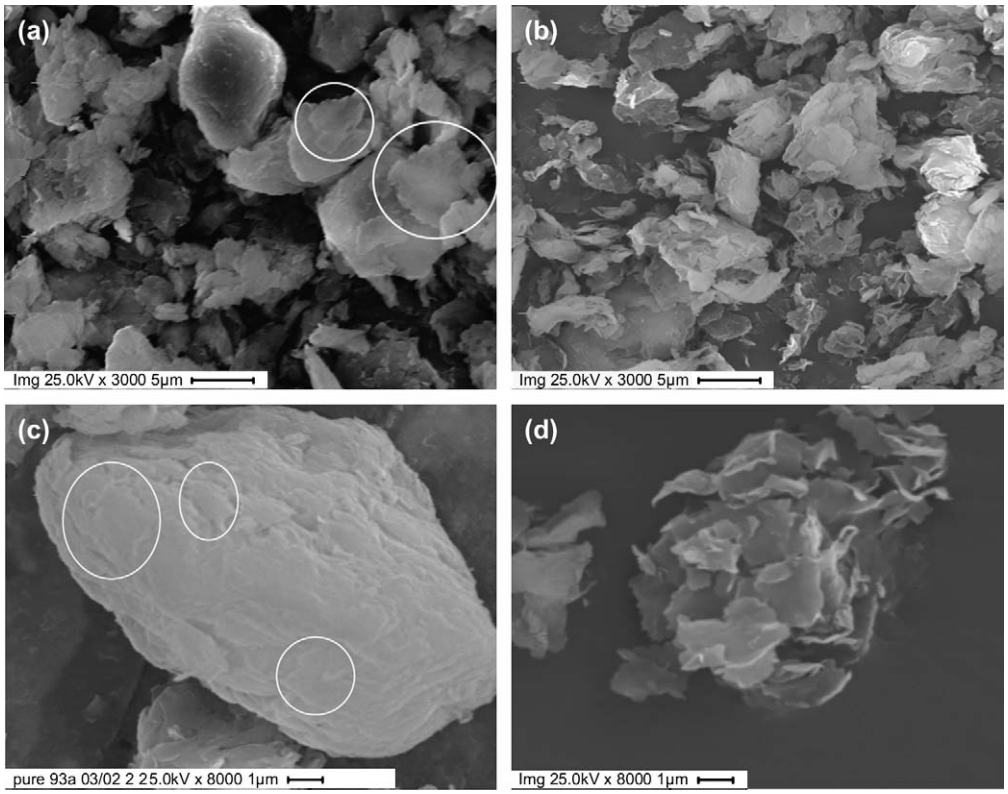

Fig. 2. SEM images of (a) as-received Cloisite 93A reveals the presence of large tightly packed particles, (b) $scCO_2$ processed Cloisite 93A with significant structural change by comparison with non processed clay, (c) as-received Cloisite 93A viewed at higher magnification and (d) $scCO_2$ processed Cloisite 93A viewed at higher magnification. Magnification and scale are present on individual images.

3. Results and discussion

3.1. Morphology of as-received and $scCO_2$ dispersed nano-clays

3.1.1. Morphology of as-received nano-clays

SEM images of the *as-received* nano-clays showed a mixture of particle sizes ranging from 1 to 15 μm. The larger particles (5–15 μm) appear to consist of many tightly bound tactoids, which align to form ellipsoidal shaped agglomerations (Figs. 2a, c, 3a, 4a, and 5a). The tactoids that make up these agglomerations have many platelets displaying good parallel registry within a given tactoid and relative to neighboring tactoids (highlighted by white circles in Figs. 2c and 3a). The smaller particles appear to consist of relatively few tactoids. However, these tactoids contain enough platelets to allow the structure to remain rigid or relatively flat even though they have the lateral dimensions of 1–5 μm (highlighted in Fig. 2a by white circles). The 'estimated' overall particle size distributions of the different nano-clays, as revealed by the examination of many SEM images, are similar. In general, all the *as-received* nano-clays consist of large tactoid structures, with very few individual platelets present.

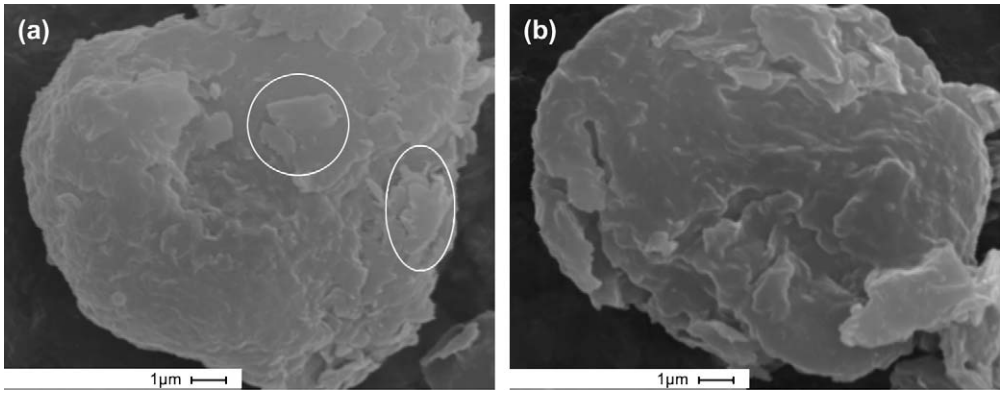

Fig. 3. SEM images of (a) as-received Cloisite 15A and (b) $scCO_2$ processed clay (90 °C, 8.6 MPa, quiescent conditions, 20 h). No changes occur during processing. The images are at a magnification of 8000.

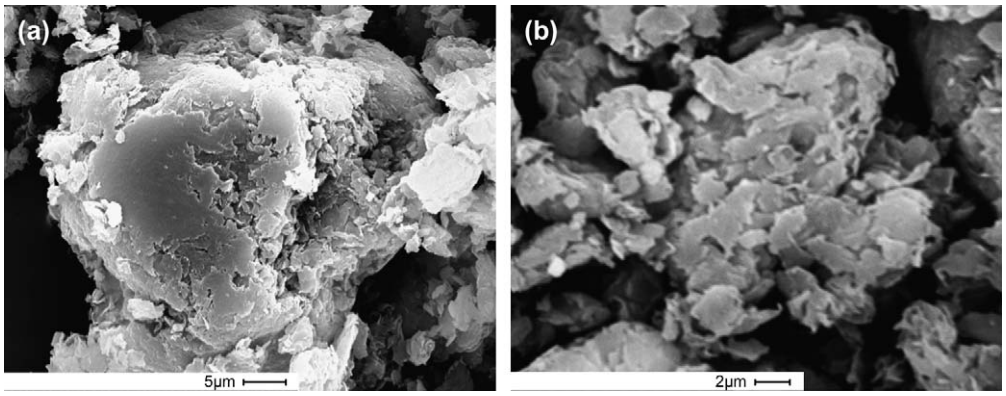

Fig. 4. SEM images of (a) as-received I.30P and (b) $scCO_2$ processed I.30P (90 °C, 8.6 MPa, quiescent conditions, 20 h). The larger ellipsoidal particles appear to be broken up into more individual tactoids.

The basal spacing of the nano-clays was determined with WAXD. The d_{001} spacing for *as-received* Cloisite 93A, Cloisite 15A, Cloisite Na^+, and I.30P was determined to be 2.4 nm, 3.1 nm, 1.2 nm, and 2.3 nm, respectively. These values are nearly identical with those published by Southern Clay Products and Nanocor (Table 1). Moreover, WAXD of Cloisite 93A, Cloisite 15A, and I.30P revealed well-defined d_{001} peaks and higher order d_{002} peaks (Figs. 6 and 7). This is in good accord with SEM images which revealed that these clays have many large ellipsoidal structures with well ordered tactoids [38]. In contrast, Cloisite Na^+ (natural clay) displayed a broad low intensity d_{001} diffraction peak and no higher order diffraction peaks (Fig. 8). This could be due to the smaller or more disordered structures in the natural clay, as shown previously [39].

3.1.2. Morphology of $scCO_2$ processed Cloisite 93A

SEM images of the *processed* Cloisite 93A revealed a significantly different morphology from the *as-received* nano-clay. Flexible expanded structures were observed as well as many individual platelets and smaller tactoids (Fig. 2b and d). The large ellipsoidal structures that were present in the *as-received* Cloisite 93A were separated into individual platelets, smaller tactoids, and cabbage-like (disordered) structures after $scCO_2$ processing. The cabbage-like structures and smaller tactoids exhibit substantial flexing and twisting. This type of distortion is not observed in the *as-received* clays or TEM images of intercalated or immiscible nanocomposites with large tactoids, but has been observed in many TEM images of exfoliated clay nanocomposites [39,40]. Upon examination of several images, the 'average' major axis length of the smaller tactoids and individual platelets was estimated to be ~0.5–2 μm, and those of the cabbage-like structures ranged in size from ~1 to 6 μm. The SEM images suggest that the outer layers of the larger and smaller particles are delaminated and the larger particles are fractured into smaller particles during processing. Calculating the average aspect ratio from SEM images is difficult in the *as-received* nano-clay and is further complicated in the *processed* nano-clays by the extreme flexing and twisting especially near the edges. However, SEM images show that aspect ratios remain large and range from 30 to 600 for *$scCO_2$ processed* Cloisite 93A.

WAXD scans of *processed* Cloisite 93A reveals the presence of a broad low intensity d_{001} diffraction peak, which corresponds to a basal spacing of 2.2 nm (Fig. 6). The broadening of the d_{001} diffraction peak and the reduction in intensity correlate well with the SEM images of this sample. The considerable loss of parallel registry and reduction in tactoid size, as a result of *$scCO_2$ processing*, explain the reduction in intensity, which is proportional to the number of coherent scattering

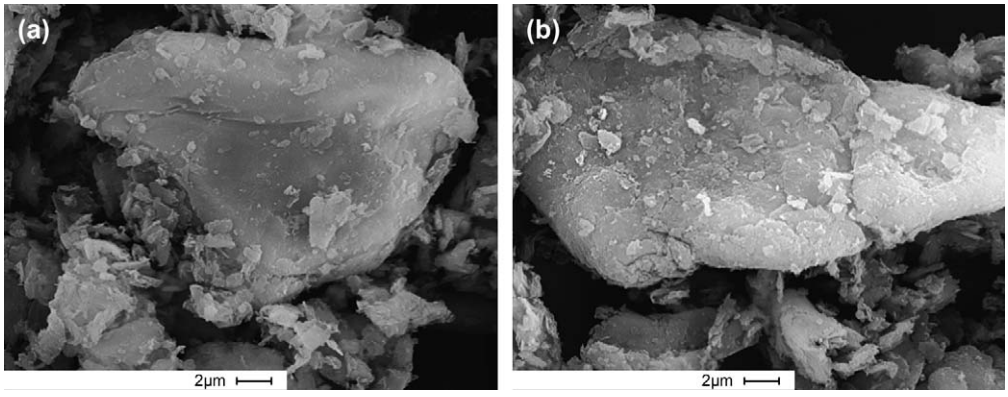

Fig. 5. SEM images of (a) as-received Cloisite Na^+ and (b) $scCO_2$ processed Cloisite Na^+ (90 °C, 8.6 MPa, quiescent conditions, 20 h). No notable changes occur during processing. The images are at a magnification of 4000.

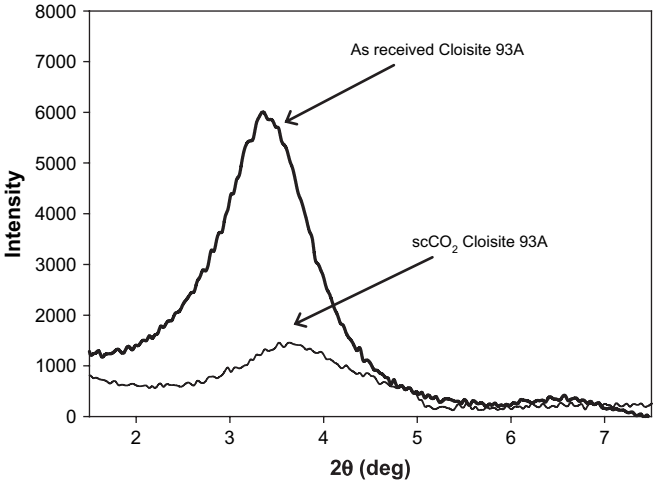

Fig. 6. WAXD of as-received Cloisite 93A and $scCO_2$ processed 93A (20 h at 8.6 MPa and 90 °C followed by rapid depressurization). A significantly lower intensity is observed for the processed clay indicating substantial reduction in the number of tactoids present. XRD was performed for the same mass of sample loaded in the same sample holder. The intensity of the processed sample is approximately a factor of 6 lower than the as-received sample. The slight shift to higher Bragg angle in the processed sample peak is attributed to the removal of some portion of the organic modifier.

points. The slight decrease in basal spacing (from 2.4 nm to 2.2 nm) of the remaining tactoids may be attributed to the removal of excess modifier from the nano-clay surface.

3.1.3. Morphology of $scCO_2$ processed Cloisite 15A, Cloisite Na^+ and I.30P

Surprisingly, SEM images of *$scCO_2$ processed* Cloisite 15A under identical conditions, revealed no significant morphology change when compared with the *as-received* clay (Fig. 3). WAXD patterns are nearly identical (not shown for brevity) for Cloisite 15A before and after *$scCO_2$* processing. Similar

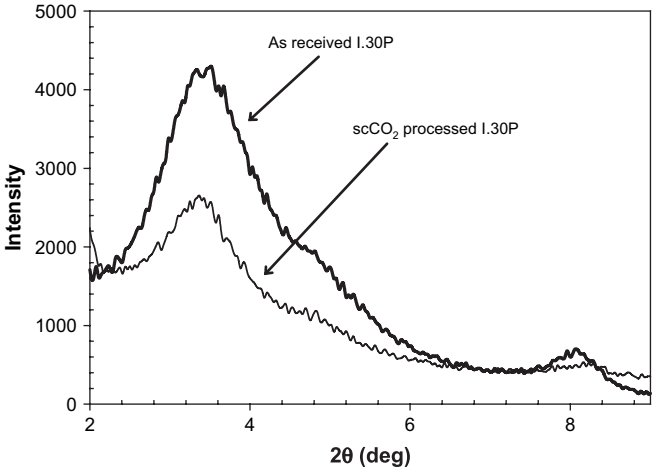

Fig. 7. WAXD of as-received and $scCO_2$ processed I.30P (20 h at 8.6 MPa and 90 °C followed by rapid depressurization). The processed clay has a lower intensity diffraction peak indicating a reduction in the number of tactoids. And the higher order peak is absent in the processed sample indicating a loss of order.

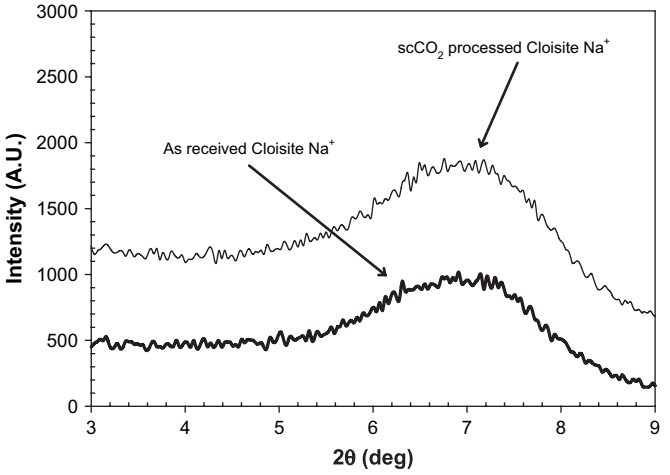

Fig. 8. WAXD of as-received Cloisite Na^+ and $scCO_2$ processed Cloisite Na^+ (20 h at 8.6 MPa and 90 °C followed by rapid depressurization). The intensity of the d_{001}-diffraction peaks is the same in both samples indicating that processing did not reduce the number of tactoids. The Bragg angle of the processed clay shifted slightly higher as a result of water removal during processing.

to Cloisite 15A, SEM images of *$scCO_2$ processed* Cloisite Na^+ (natural clay) revealed that the particles were largely unchanged by processing at comparable conditions (Fig. 5). The large ellipsoidal particles remained after processing and appeared well ordered like those of the *as-received* clay. WAXD scans of *$scCO_2$ processed* Cloisite Na^+ correlate well with the SEM images (Fig. 8). The intensity and breadth of the d_{001} diffraction peaks for the *as-received* and the *$scCO_2$ processed* Cloisite Na^+ are nearly identical, indicating no dispersion has been achieved. In contrast, SEM images of *$scCO_2$ processed* I.30P show a moderate amount of dispersion when compared to the *as-received* and *processed* clay (Fig. 4). The large ellipsoidal particles are partially reduced in size with the larger remaining particles estimated to be ranging from ~2 to 5 μm rather than 10–25 μm. The surfaces of the particles appear to have become disordered similar to those of *$scCO_2$ processed* Cloisite 93A but to a lesser extent. WAXD data for the *$scCO_2$ processed* I.30P shows a reduced intensity and broadened d_{001} diffraction peak (Fig. 7). This is reasonable given the structural changes seen in SEM images of this sample.

3.1.4. Discussion of $scCO_2$ processed nano-clay dispersion results

Two of the nano-clays were dispersed to varying extents via *$scCO_2$ processing*, Cloisite 93A was well dispersed and I.30P was moderately dispersed. In contrast, Cloisite 15A and Cloisite Na^+ demonstrated no significant morphological change after *$scCO_2$ processing* at comparable conditions. The key differences between the nano-clays are inter-gallery spacing and composition of the ammonium salts. The inter-gallery spacing does not appear to be a limiting factor among the modified nano-clays, as Cloisite 15A is virtually unaffected by the *$scCO_2$* process and has the largest of the inter-gallery spacing. The key difference between the structure of Cloisite 15A and

Cloisite 93A is that a methyl group in 15A is replaced with an acidic hydrogen in 93A. The acidic hydrogen content of Cloisite 93A *may* be the key reason for the difference in CO_2-philicity between the two clays. This assumption appears reasonable when considering previous work which has suggested that the CO_2 solubility of imidazolium-based ionic salts increased if a hydrogen was present on the salt rather than a methyl group for the solvent to interact with [41,42]. Additionally, Brennecke et al. demonstrated a slightly increased CO_2 solubility of imidazolium salts, when hydrogen was substituted for a methyl group on the C2 position of the ring [43].

The ability to moderately disperse I.30P via *$scCO_2$ processing* and not Cloisite 15A cannot be explained by an acidic hydrogen. A preliminary hypothesis is given here. In imidazolium salts, it has been shown that at higher pressures CO_2 will act favorably with the higher positive charge on the N, which results when methyl groups are present near the N3 nitrogen [43]. Further evidence of this behavior is provided by Deschamps et al. who demonstrated by molecular simulation that increasing the positive charge on the N increases CO_2 activity in the region close to the N [44]. In the case of I.30P, there are three methyl groups surrounding the N rather than two for Cloisite 15A. In addition, if one considers that Cloisite 15A has an additional hydrogenated tallow group it likely has the ability to distribute the charge associated with the quaternary ammonium salt over a larger area, effectively lowering the local charge around the N. The lower aliphatic content of I.30P compared with Cloisite 15A along with the increase of methyl groups likely results in an increased positive charge on the N of I.30P. The increased positive nature of the N in I.30P may explain the apparent difference in CO_2-philicity and dispersion of I.30P and Cloisite 15A.

In the case of Cloisite Na^+, the closely packed platelets (smaller *d*-spacing compared to other clays), and charge repulsion due to the charged clay surface, may have prevented $scCO_2$ from effectively diffusing into the gallery resulting in no separation of the individual platelets during depressurization. Interestingly, in the presence of a CO_2-philic polymer (PDMS) some dispersion of Cloisite Na^+ was achieved (discussed later in nanocomposite section).

In summary, although the fundamental reasons for the differences in dispersion of the nano-clays are not entirely clear, two structural features appear to play a role: (1) the presence of an acidic hydrogen on the ammonium salt and (2) the extent of the positive charge on the N. The presence of acidic hydrogen or the increased positive nature of the N appears to render the clay more CO_2-philic resulting in better dispersion of Cloisite 93A and I.30P.

3.2. PDMS Cloisite Na^+ nanocomposites

3.2.1. Preparation and structure of Cloisite Na^+/PDMS nanocomposites

In the previous section, we described the ability of *$scCO_2$ processing* to disperse 'CO_2-philic' nano-clays. Here we provide evidence that a CO_2-philic polymer (PDMS) can be used to disperse 'CO_2-phobic' Cloisite Na^+ (as-received natural clay). Initially, a blend of low molecular weight (39K) PDMS and high molecular weight (400K) PDMS was used to prepare the natural montmorillonite-based nanocomposites. The low molecular weight PDMS was used to increase the mobility and improve the chances of PDMS to diffuse into the clay galleries. This was based on the results of DeSimone et al. who demonstrated that the diffusivity of PDMS in CO_2 scaled as the inverse square of molecular weight and that solubility increased as the molecular weight decreased [37].

The first nanocomposite, sample ($PDMS_{blend}$(sc)) was formed by blending 15 wt% *as-received* Cloisite Na^+ with the PDMS mixture and processing the resulting composite in *$scCO_2$*. TEM images reveal regions of aggregated clay and some dispersed/exfoliated clay. The aggregated regions appear to comprise tactoids consisting of 20 or fewer layers (Fig. 9) which is significantly fewer layers than SEM images reveal for *as-received* Cloisite Na^+ (Fig. 5a). In addition, considering that the largest dimension of the aggregated clay areas is typically less than 5 μm, it appears that the majority of the larger particles have been broken up into smaller tactoids. The light grey regions seen in the images comprise individual platelets or small tactoids and the black regions comprise disordered intercalated structures, tactoids, and partially exfoliated structures. X-ray scans of sample ($PDMS_{blend}$(sc)) lack a coherent d_{001} diffraction peak and are consistent with a dispersed or partially dispersed nanocomposites (Fig. 10). In comparison, the WAXD results of the melt-annealed sample ($PDMS_{400K}$(BM)) showed a well-defined d_{001} diffraction peak (Fig. 14) at comparable clay loadings. Therefore, the $scCO_2$ processing appears to have produced appreciable clay dispersion, consistent with TEM images. Morgan and Gilman have suggested that WAXD may become insensitive to the clay morphology at loadings of less than 5 wt% and at these low loadings coherent diffraction peaks may not be present even when the clay remains primarily in tactoid form [39]. This is one of the reasons why we chose to use a relatively high clay loading of 15%. Thus it appears that a CO_2-philic polymer (PDMS) enables *$scCO_2$ processing* to disperse even natural clay (Cloisite Na^+). The high diffusivity and low viscosity of the PDMS in $scCO_2$, coupled with the favorable interaction between the Si–O backbone of the PDMS and the Si–O surface of Cloisite Na^+ may have increased the ability of PDMS to penetrate the clay galleries, facilitating the transport of CO_2 into the clay galleries.

3.2.2. Viscoelastic behavior of Cloisite Na^+/PDMS nanocomposites

The viscoelastic properties of sample ($PDMS_{blend}$(sc)) showed significant increases in the dynamic moduli. The storage modulus (G') increased by ~100% at all frequencies compared to the neat polymer (Fig. 11). Furthermore, the cross-over frequency and the frequency dependence of the moduli were comparable to those of the matrix polymer. This suggests that the relaxation dynamics of the matrix polymer is largely unaffected by the presence of the dispersed nano-clay. Steady shear viscosity (η) measurements also

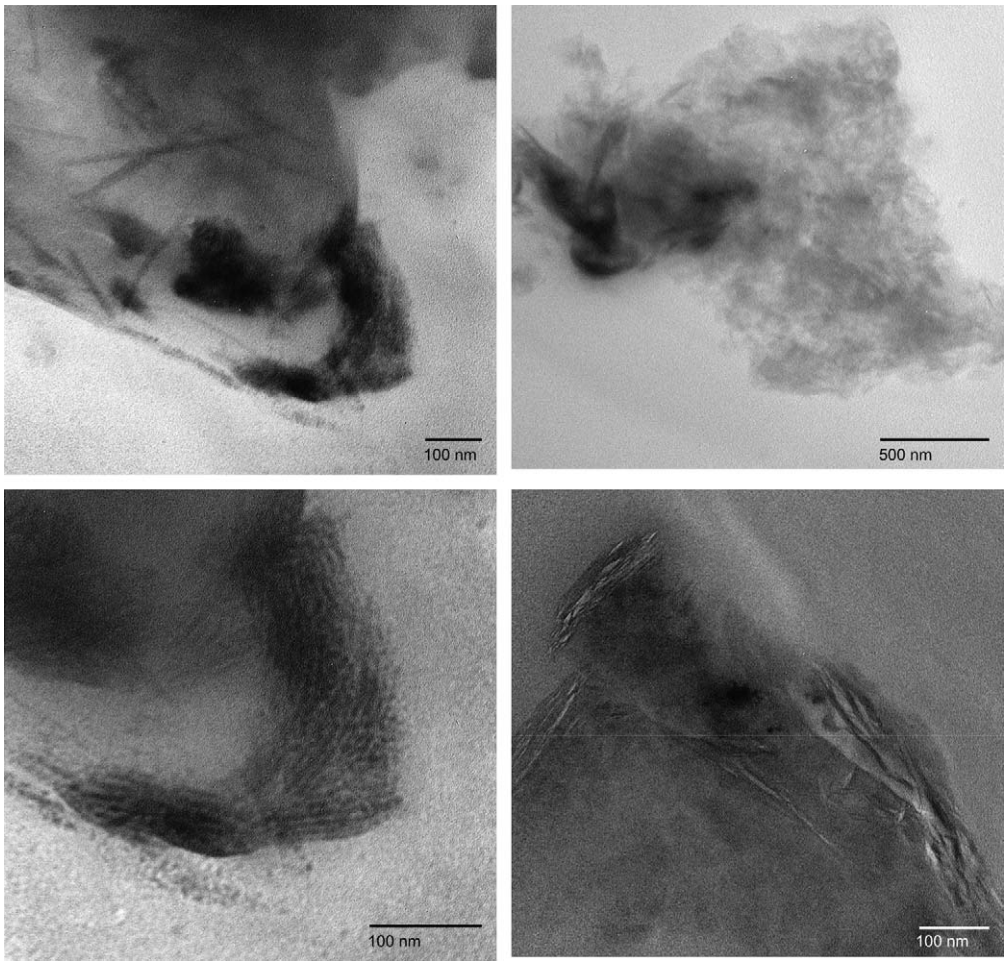

Fig. 9. TEM images of 15 wt% Cloisite Na^+ mixed with PDMS blend (20 wt% 39K, 80 wt% 400K) processed in $scCO_2$. All the scaling bars represent 100 nm except the top right image where the scaling bar represents 500 nm. Light grey regions are areas of individual platelets and tactoids. Dark regions are regions of disordered intercalated structures, partially exfoliated structures and tactoids. All images are from different regions of sample ($PDMS_{blend}$(sc)) at different magnifications.

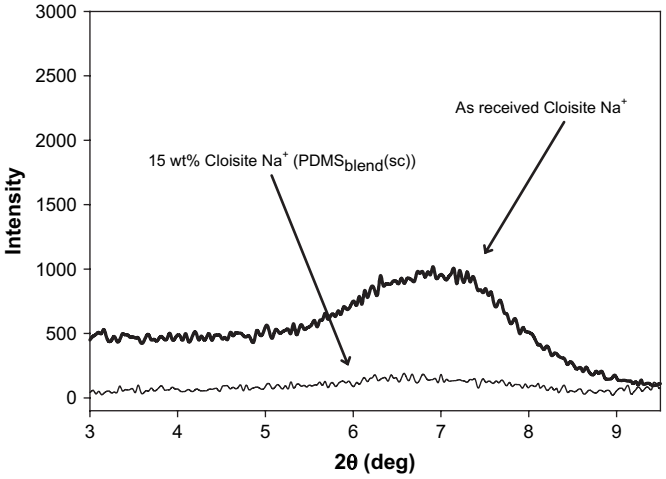

Fig. 10. WAXD scans of *as-received* Cloisite Na^+ and sample ($PDMS_{blend}$(sc)), which was formed by mixing *as-received* Cloisite Na^+ with a blend of high and low molecular weight PDMS (20 wt% 39K, 80 wt% 400K) and processing the composite in $scCO_2$ for 24 h at 13.78 MPa, and 50 °C. The absence of a coherent diffraction peak for the nanocomposite is indicative of a well dispersed system.

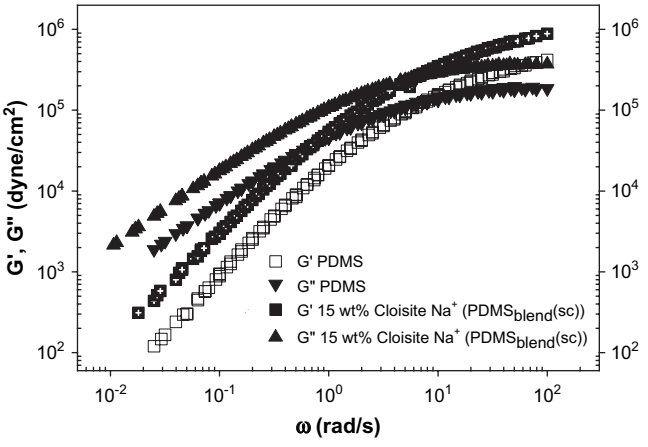

Fig. 11. Oscillatory shear rheology of neat PDMS and 15 wt% Cloisite Na^+/PDMS nanocomposite. The nanocomposite was formed by mixing *as-received* Cloisite Na^+ with a PDMS blend (20 wt% 39K, 80 wt% 400K) and processing in $scCO_2$. The nanocomposite displays a factor of 2 increase in G' and G'' across the entire frequency range but exhibits relaxation dynamics similar to the neat polymer as indicated by the lack of shift in cross-over frequency and the similar frequency dependence of the moduli.

exhibit a large increase ~170% in zero-shear viscosity, (Fig. 12) with the onset of the plateau occurring at lower shear rates for the nanocomposite. As a benchmark, when the matrix polymer blend was melt-annealed (without $scCO_2$) with Cloisite Na^+, we observed a modulus increase (at all frequencies) of ~20%. This is much smaller than that observed for $scCO_2$ *processed* nanocomposites. Krishnamoorti et al. prepared *dispersed* PDMS/organo-clay (dimethylditallow-montmorillonite) nanocomposites with a large clay-spacing compared to Cloisite Na^+, by *in situ polymerization.* They observed qualitatively similar frequency dependence and η dependence, with an increase in zero-shear viscosity of ~40% for a silicate content of 13 wt% [45]. Therefore, our results suggest that $scCO_2$ *processing* results in good clay dispersion, even for natural clays in the presence of PDMS.

Even though appreciable dispersion and modulus enhancement were observed, this sample ($PDMS_{blend}$(sc)) showed liquid-like terminal behavior. This is further supported by the plateau observed in the cross-plot (η^* vs. G^*) of the nanocomposite (Fig. 13), which is sensitive to the onset of solid-like behavior. This type of rheological response is similar to that of traditional filled systems where the relaxation dynamics of the host polymer is unaltered by the presence of the non-interacting filler. Typically, dispersed nanocomposites display an alteration in relaxation dynamics seen as a plateau in G' at low frequencies. This is attributed to the coupling of the host matrix to a percolated clay network [45]. The lack of a plateau in G' for sample ($PDMS_{blend}$(sc)) is surprising because the Si–O backbone of PDMS and the Si–O surface of the natural clay should interact favorably (especially since this polymer enabled natural clay to be dispersed). One possible explanation for the lack of a plateau in the dispersed $PDMS_{blend}$(sc) could be the presence of low molecular weight PDMS in the host matrix. Compared to the high molecular weight PDMS (400K), it is estimated to be significantly more soluble in

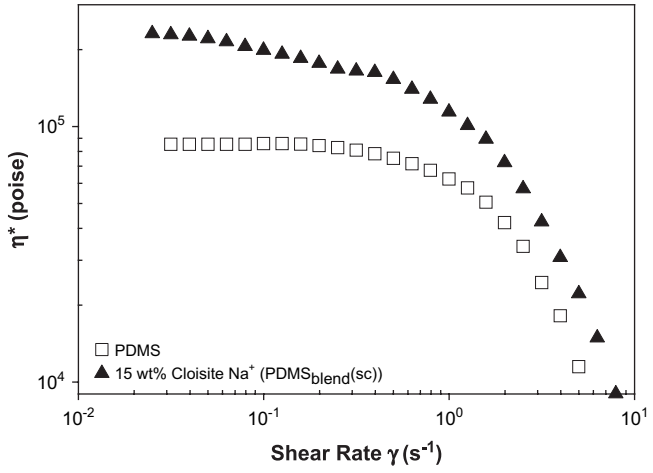

Fig. 12. Steady shear viscosity of neat PDMS and 15 wt% Cloisite Na^+/PDMS nanocomposite. The nanocomposite was formed by mixing *as-received* Cloisite Na^+ with a PDMS blend (20 wt% 39K, 80 wt% 400K) and processing in $scCO_2$. The nanocomposite exhibits a steady shear viscosity increase of 170% and the low shear rate plateau occurs at a lower shear rate compared with the neat polymer.

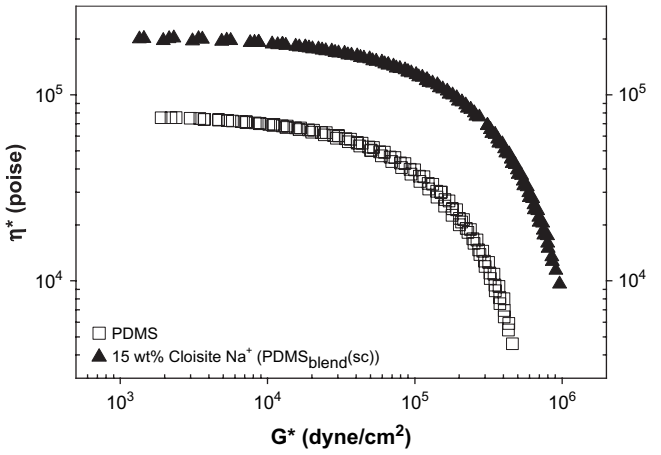

Fig. 13. Cross-plot of neat PDMS and 15 wt% Cloisite Na^+/PDMS nanocomposite. The nanocomposite was formed by mixing *as-received* Cloisite Na^+ with a PDMS blend (20 wt% 39K, 80 wt% 400K) and processing in $scCO_2$. The nanocomposite exhibits a finite dynamic viscosity over the range of complex moduli.

CO_2 and has a 100-fold higher diffusivity [37]. Therefore, it may be transported to the clay surface preferentially. If a substantial portion of the clay surface is coated with the low molecular weight PDMS, the tethered chains may not be long enough to 'couple' with the matrix, resulting in a filler effect.[3]

To test this idea, a nanocomposite was formed using only the 400K molecular weight PDMS. The sample ($PDMS_{400K}$(sc)) was made by processing *as-received* Cloisite Na^+ mixed with PDMS (400K) in $scCO_2$. *In order to disperse the Cloisite Na^+ with the higher molecular weight PDMS, it was necessary to increase the processing pressure from 13.78 MPa to 27.6 MPa, maintaining the same temperature of 50 °C.*[4] WAXD data for sample ($PDMS_{400K}$(sc)) indicate that the Cloisite Na^+ was well dispersed (Fig. 14). The sample was then benchmarked against sample ($PDMS_{400K}$(BM)) which was prepared by mechanically mixing the *as-received* Cloisite Na^+ with high molecular weight PDMS and annealing for 24 h in a vacuum oven at 90 °C. X-ray scans of this melt-mixed sample revealed a lack of clay dispersion (Fig. 14).

The dynamic moduli of the sample ($PDMS_{400K}$(sc)) demonstrate significant improvement across the measured frequency range, with better improvement at low frequencies compared to high frequencies (Fig. 15). G' is enhanced by ~100% at high frequencies, and more than an order of magnitude at low frequencies. Importantly, a low frequency plateau is present in G' suggesting a network formation in the dispersed nanocomposite [25]. This is in contrast to the previous 'blend' sample ($PDMS_{blend}$(sc)), which showed no low frequency plateau. Furthermore, η^* is considerably enhanced at all frequencies and exhibits shear thinning across the entire measured frequency range with strong shear

[3] Even if we assume that 66% of the clay is dispersed into individual platelets, our estimates suggest that 20% of low molecular weight PDMS (39K) is sufficient to coat the clay layers.

[4] We attempted to process the blend sample at these higher pressures, but some PDMS was lost during processing, presumably the highly soluble low molecular weight fraction.

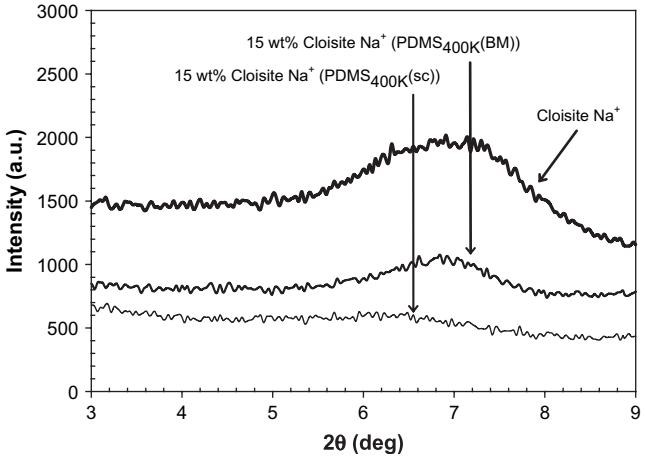

Fig. 14. WAXD scans of *as-received* Cloisite Na^+, sample ($PDMS_{400K}$(BM)), and sample ($PDMS_{400K}$(sc)). Sample ($PDMS_{400K}$(BM)) was formed by mixing 15 wt% *as-received* Cloisite Na^+ with high molecular weight PDMS and annealing the resulting composite at 90 °C in a vacuum oven for 24 h. The d_{001} diffraction peak for sample ($PDMS_{400K}$(BM)) has the same FWHM as the *as-received* Cloisite Na^+ indicating no dispersion. Sample ($PDMS_{400K}$(sc)) was formed by mixing 15 wt% *as-received* Cloisite Na^+ with high molecular weight PDMS and processing in $scCO_2$. The lack of a coherent d_{001} diffraction peak is indicative of a well dispersed nanocomposite.

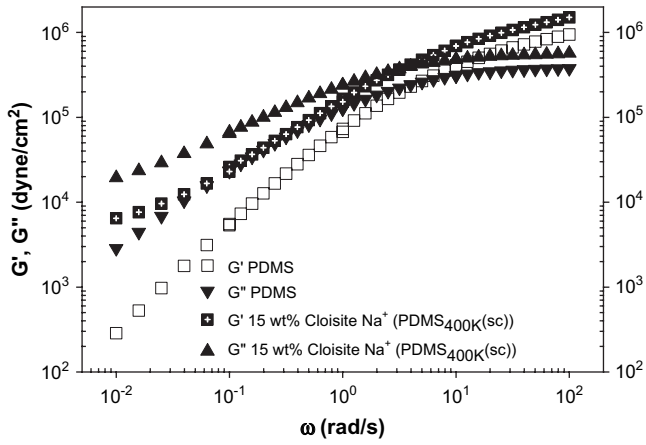

Fig. 15. Oscillatory shear rheology of neat PDMS and 15 wt% Cloisite Na^+/PDMS nanocomposite ($PDMS_{400K}$(sc)). The nanocomposite was formed by mixing *as-received* Cloisite Na^+ with high molecular weight PDMS and processing in $scCO_2$. The nanocomposite displays a factor of 2 increase in G' and G'' at high frequencies and more than an order of magnitude in G' at low frequencies. Furthermore, the nanocomposite exhibits the onset of a plateau in G' at low frequencies.

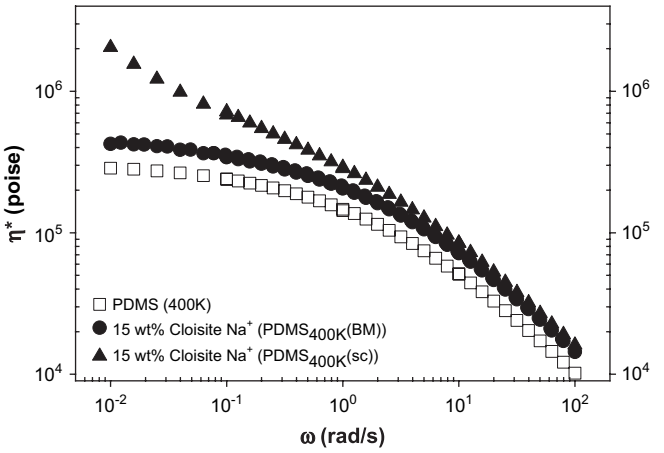

Fig. 16. Complex viscosity of neat PDMS, sample $PDMS_{400K}$(BM), and sample $PDMS_{400K}$(sc). Sample $PDMS_{400K}$(BM) was formed by mixing 15 wt% *as-received* Cloisite Na^+ with high molecular weight PDMS and annealing the resulting composite at 90 °C in a vacuum oven for 24 h. The nanocomposite was formed by mixing *as-received* Cloisite Na^+ with high molecular weight PDMS and processing in $scCO_2$. The plot demonstrates shear thinning behavior for the $scCO_2$ *processed* nanocomposite even at the lowest frequencies measured. This type of behavior is typical of dispersed nanocomposite with good polymer/clay interactions.

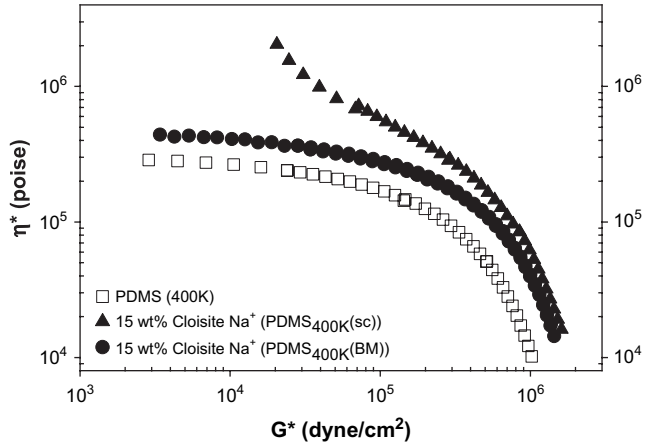

Fig. 17. Cross-plot of neat PDMS, sample $PDMS_{400K}$(BM), and sample $PDMS_{400K}$(sc). Sample $PDMS_{400K}$(BM) was formed by mixing 15 wt% *as-received* Cloisite Na^+ with high molecular weight PDMS and annealing the resulting composite at 90 °C in a vacuum oven for 24 h. The nanocomposite was formed by mixing *as-received* Cloisite Na^+ with high molecular weight PDMS and processing in $scCO_2$. The plot demonstrates the solid-like behavior of the nanocomposite as seen by the divergence of complex viscosity at large finite values of G^*. This type of behavior is typical of dispersed nanocomposite with good polymer/clay interactions.

thinning prevalent even at low frequencies (Fig. 16). The benchmark sample ($PDMS_{400K}$(BM)) did not show this behavior. A cross-plot reveals the divergence of η^* at finite values of G^* which is indicative of the solid-like nature exhibited by some exfoliated nanocomposites with good polymer/clay interactions (Fig. 17) [25]. Even though both $scCO_2$ processed samples ($PDMS_{blend}$(sc)) and ($PDMS_{400K}$(sc)) show comparable dispersion based on WAXD, the latter sample shows a low frequency plateau whereas the former does not. The reason for this is not clear, and we offer this preliminary hypothesis: the length of the clay-adsorbed chain may play an important role in (a) creating a percolated clay structure connecting adjacent 'dispersed' layers, and/or (b) coupling the 'matrix polymer dynamics' to the clay layer. If this were the case, the 400K PDMS should have promoted clay/polymer interactions in the blend sample too. The fact that no such solid-like behavior is seen, suggests that when 39K PDMS is present it could be adsorbing on the clay surface preferentially in the blend. This may be reasonable, since 20% of low molecular weight PDMS is ample to coat the clay surface (estimate based

on ~70% dispersion) in the blend, and because of its higher solubility and significantly increased diffusivity in $scCO_2$ [37].

4. Conclusions

We investigated *$scCO_2$*-based dispersion of nano-clays and polymer nanocomposites. The structure and the properties of the resultant materials were characterized using a combination of WAXD, SEM, TEM and rheology. Our results indicate that nano-clays can be delaminated by the *$scCO_2$ process* and the extent of dispersion is dependent on the CO_2-philicity of the nano-clay. Significant dispersion was achieved with Cloisite 93A, whereas relatively little dispersion was achieved for Cloisite Na^+ (natural clay). It appears that the presence of acidic hydrogen on the ammonium salt (as in the case of 93A) or an increased positive charge on the N of the ammonium salt (I.30P) may improve the CO_2-philicity of the nano-clay, thereby increasing dispersion. In addition, results demonstrate that natural clay can be dispersed by combining CO_2-philic PDMS with the clay prior to processing. The resultant dispersed Cloisite Na^+/PDMS nanocomposite had significant enhancements in the rheological properties, and showed a solid-like low frequency plateau, characteristic of dispersed nanocomposites with good polymer/clay interactions. Therefore, other CO_2-philic polymers may be capable of dispersing natural clay, which could lead to superior nanocomposites at a reduced cost.

Acknowledgments

Funding from NSF (DMR 9876221 and CTS 0335315) and WSU-Institute of Manufacturing Research are greatly appreciated. We would also like to thank Professor Charles Manke for providing us access to the Rheometrics ARES rheometer.

References

[1] Kojima Y, Usuki A, Kawasumi M, Okada A, Kurauchi T, Kamigaito O. One-pot synthesis of nylon 6-clay hybrid. Journal of Polymer Science Part A: Polymer Chemistry 1993;31(7):1755–8.
[2] Messersmith PB, Giannelis EP. Synthesis and characterization of layered silicate–epoxy nanocomposites. Chemistry of Materials 1994;6(10): 1719–25.
[3] Kojima Y, Fukumori K, Usuki A, Okada A, Kurauchi T. Gas permeabilities in rubber–clay hybrid. Journal of Materials Science Letters 1993; 12(12):889–90.
[4] Gilman JW, Kashiwagi T, Lichtenhan JD. Nanocomposites: a revolutionary new flame retardant approach. SAMPE Journal 1997;33(4):40–6.
[5] Giannelis EP. Polymer layered silicate nanocomposites. Advanced Materials (Weinheim, Germany) 1996;8(1):29–35.
[6] Giannelis EP. Polymer-layered silicate nanocomposites: synthesis, properties and applications. Applied Organometallic Chemistry 1998;12(10/11): 675–80.
[7] Giannelis EP, Krishnamoorti R, Manias E. Polymer–silicate nanocomposites: model systems for confined polymers and polymer brushes. Advances in Polymer Science 1999;138:107–47.
[8] Gilman JW. Flammability and thermal stability studies of polymer layered-silicate (clay) nanocomposites. Applied Clay Science 1999; 15(1–2):31–49.
[9] Gilman JW, Jackson CL, Morgan AB, Harris Jr R, Manias E, Giannelis EP, et al. Flammability properties of polymer-layered silicate nanocomposites. Polypropylene and polystyrene nanocomposites. Chemistry of Materials 2000;12(7):1866–73.
[10] Kojima Y, Usuki A, Kawasumi M, Okada A, Kurauchi T, Kamigaito O. Synthesis of nylon 6-clay hybrid by montmorillonite intercalated with e-caprolactam. Journal of Polymer Science Part A: Polymer Chemistry 1993;31(4):983–6.
[11] Messersmith PB, Giannelis EP. Synthesis and barrier properties of poly(e-caprolactone)-layered silicate nanocomposites. Journal of Polymer Science Part A: Polymer Chemistry 1995;33(7):1047–57.
[12] Usuki A, Kojima Y, Kawasumi M, Okada A, Fukushima Y, Kurauchi T, et al. Synthesis of nylon 6-clay hybrid. Journal of Materials Research 1993;8(5):1179–84.
[13] Vaia RA, Price G, Ruth PN, Nguyen HT, Lichtenhan J. Polymer/layered silicate nanocomposites as high performance ablative materials. Applied Clay Science 1999;15(1–2):67–92.
[14] Zhu J, Morgan AB, Lamelas FJ, Wilkie CA. Fire properties of polystyrene–clay nanocomposites. Chemistry of Materials 2001;13(10): 3774–80.
[15] Blumstein A. Polymerization of adsorbed monolayers. II. Thermal degradation of the inserted polymer. Journal of Polymer Science Part A: General Papers 1965;3(7):2665–72.
[16] Aranda P, Ruiz-Hitzky E. Poly(ethylene oxide)–silicate intercalation materials. Chemistry of Materials 1992;4(6):1395–403.
[17] Burnside SD, Giannelis EP. Synthesis and properties of new poly(dimethylsiloxane) nanocomposites. Chemistry of Materials 1995;7(9): 1597–600.
[18] Fornes TD, Yoon PJ, Keskkula H, Paul DR. Nylon 6 nanocomposites: the effect of matrix molecular weight. Polymer 2001;42(25):09929–40.
[19] Lepoittevin B, Pantoustier N, Devalckenaere M, Alexandre M, Kubies D, Calberg C, et al. Poly(e-caprolactone)/clay nanocomposites by in-situ intercalative polymerization catalyzed by dibutyltin dimethoxide. Macromolecules 2002;35(22):8385–90.
[20] Ray SS, Okamoto M. Polymer/layered silicate nanocomposites: a review from preparation to processing. Progress in Polymer Science 2003; 28(11):1539–641.
[21] Vaia RA, Giannelis EP. Polymer melt intercalation in organically-modified layered silicates: model predictions and experiment. Macromolecules 1997;30(25):8000–9.
[22] Vaia RA, Ishii H, Giannelis EP. Synthesis and properties of two-dimensional nanostructures by direct intercalation of polymer melts in layered silicates. Chemistry of Materials 1993;5(12):1694–6.
[23] Vaia RA, Jandt KD, Kramer EJ, Giannelis EP. Kinetics of polymer melt intercalation. Macromolecules 1995;28(24):8080–5.
[24] Weimer MW, Chen H, Giannelis EP, Sogah DY. Direct synthesis of dispersed nanocomposites by in situ living free radical polymerization using a silicate-anchored initiator. Journal of the American Chemical Society 1999;121(7):1615–6.
[25] Xu L, Reeder S, Thopasridharan M, Ren J, Shipp DA, Krishnamoorti R. Structure and melt rheology of polystyrene-based layered silicate nanocomposites. Nanotechnology 2005;16(7):514–21.
[26] Kirby CF, McHugh MA. Phase behavior of polymers in supercritical fluid solvents. Chemical Reviews (Washington, D.C.) 1999;99(2): 565–602.
[27] Panza JL, Beckman EJ. Supercritical fluid technology in materials science and engineering. Marcel Dekker; 2002.
[28] Tomasko DL, Li H, Liu D, Han X, Wingert MJ, Lee LJ, et al. A review of CO_2 applications in the processing of polymers. Industrial and Engineering Chemistry Research 2003;42(25):6431–56.
[29] Consani KA, Smith RD. Observations on the solubility of surfactants and related molecules in carbon dioxide at 50 °C. Journal of Supercritical Fluids 1990;3(2):51–65.
[30] Harris TV, Irani CA, Pretzer WR. US Patent 5,045,220, September 3, 1991.
[31] Hoefling TA, Newman DA, Enick RM, Beckman EJ. Effect of structure on the cloud-point curves of silicone-based amphiphiles in supercritical carbon dioxide. Journal of Supercritical Fluids 1993;6(3):165–71.
[32] McHugh MA, Krukonis V. Supercritical fluid extraction. 2nd ed. Boston, MA: Butterworth–Heinemann; 1994.

[33] Gulari E, Serhatkulu G, Kannan RM. Method for delaminating aggregated particles with a coating agent in a substantially supercritical fluid. Patent pending; 2004.
[34] Manke CW, Gulari E, Mielewski DF, Lee ECC. US Patent 6,469,073, October 22, 2002.
[35] Gerhardt LJ, Garg A, Manke CW, Gulari E. Concentration-dependent viscoelastic scaling models for polydimethylsiloxane melts with dissolved carbon dioxide. Journal of Polymer Science Part B: Polymer Physics 1998;36(11):1911–8.
[36] Kwag C, Manke CW, Gulari E. Rheology of molten polystyrene with dissolved supercritical and near-critical gases. Journal of Polymer Science Part B: Polymer Physics 1999;37(19):2771–81.
[37] Royer JR, DeSimone JM, Khan SA. Carbon dioxide-induced swelling of poly(dimethylsiloxane). Macromolecules 1999;32(26):8965–73.
[38] Cullity BD, Stock SR. Elements of X-ray diffraction. 3rd ed. Pearson Education; 2001.
[39] Morgan AB, Gilman JW. Characterization of polymer-layered silicate (clay) nanocomposites by transmission electron microscopy and X-ray diffraction: a comparative study. Journal of Applied Polymer Science 2003;87(8):1329–38.
[40] Plummer CJG, Garamszegi L, Leterrier Y, Rodlert M, Maanson J-AE. Hyperbranched polymer layered silicate nanocomposites. Chemistry of Materials 2002;14(2):486–8.
[41] Aki SNVK, Mellein BR, Saurer EM, Brennecke JF. High-pressure phase behavior of carbon dioxide with imidazolium-based ionic liquids. Journal of Physical Chemistry B 2004;108(52):20355–65.
[42] Crowhurst L, Mawdsley PR, Perez-Arlandis JM, Salter PA, Welton T. Solvent–solute interactions in ionic liquids. Physical Chemistry Chemical Physics 2003;5(13):2790–4.
[43] Cadena C, Anthony JL, Shah JK, Morrow TI, Brennecke JF, Maginn EJ. Why is CO_2 so soluble in imidazolium-based ionic liquids? Journal of the American Chemical Society 2004;126(16):5300–8.
[44] Deschamps J, Costa Gomes Margarida F, Padua Agilio AH. Molecular simulation study of interactions of carbon dioxide and water with ionic liquids. Chemphyschem: a European journal of chemical physics and physical chemistry 2004;5(7):1049–52.
[45] Krishnamoorti R, Vaia RA, Giannelis EP. Structure and dynamics of polymer-layered silicate nanocomposites. Chemistry of Materials 1996;8(8):1728–34.